J. Fluid Mech. (1969), *vol.* 35, *part* 4, *pp.* 775–798
Printed in Great Britain

Instabilities of a buoyancy-driven system

By A. E. GILL

Department of Applied Mathematics and Theoretical Physics,
University of Cambridge

AND A. DAVEY

National Physical Laboratory, Teddington, Middlesex

(Received 16 May 1968)

A buoyancy-driven system can be unstable due to two different mechanisms—one mechanical and the other involving buoyancy forces. The mechanical instability is of the type normally studied in connexion with the Orr–Sommerfeld equation. The buoyancy-driven instability is rather different and is related to the 'Coriolis'-driven instability of rotating fluids. In this paper, the stability of a buoyancy-driven system, recently called a 'buoyancy layer', is examined for the whole range of Prandtl numbers, σ. The buoyancy-driven instability becomes increasingly important as the Prandtl number is increased and so particular interest is attached to the limit in which the Prandtl number tends to infinity. In this limit, the system is neutrally stable to first order, but second-order effects render the flow unstable at a Reynolds number of order $\sigma^{-\frac{1}{2}}$. Consequences of the results for the stability of convection in a vertical slot are examined.

1. Introduction

This paper contains a study of the stability, to two-dimensional disturbances, of a temperature and flow field established as a result of natural convection. It is not *just* the study of a flow field as it will be seen that the basic temperature field plays an important part in producing instabilities. This is because temperature fluctuations derived from the basic temperature field result in the action of buoyancy forces, which can only be ignored in certain limiting cases. Buoyancy is, in fact, found to be the major source of instability in near-critical conditions unless the Prandtl number is small.

The particular system chosen for study is an exact solution of the equations of motion (to the Boussinesq approximation). The velocity is unidirectional and depends only on a single co-ordinate x_*. The temperature, relative to a state of uniform stratification, is also a function of x_* only, and the basic solution can be expressed in a form which does not involve the Prandtl number. The solution is a special case of a solution obtained by Prandtl (1952, p. 422) for 'mountain and valley winds'. It is discussed by Gill (1966) in connexion with natural convection in a rectangular cavity at large Rayleigh numbers and found to be an approximation to the solution in the boundary layers on the vertical walls of the cavity. The solution is also discussed by Veronis (1967) and Barcilon & Pedlosky (1967)

and shown to be of importance in the study of strongly stratified systems. In this context, the boundary layer concerned is referred to as a 'bouyancy' layer.

There are thus three ways in which the present study may be useful: (*a*) as a detailed study over the whole range of Prandtl numbers of the stability of a system established by natural convection; (*b*) as a study relating to the stability of natural convection in a rectangular cavity; (*c*) as a study of the stability of a buoyancy layer.

The first study of the stability of a system driven by natural convection appears to have been made by Gershuni (1953). The system concerned was that established between infinite parallel vertical plates maintained at different fixed temperatures. A Galerkin method was used to the lowest approximation possible. The method was later refined by using more terms in the series of functions involved by Gershuni & Zhukhovitzki (1958), Kappus & Lehmann (1965) and Rudakov (1967). Gershuni (1955) also studied the case where the plates were inclined to the vertical.

Nachtsheim (1963) studied the stability of the velocity and temperature field set up by natural convection in the neighbourhood of a vertical uniform flux plate. The calculations were made for Prandtl numbers of 0·733 and 6·7 using direct integration of the relevant equations, the parallel-flow approximation having been made. He compared his results with those obtained by neglecting the temperature fluctuations, that is by neglecting the thermal source of disturbance energy. For the larger Prandtl number, the neutral stability curves obtained by the two methods were quite different. For the smaller Prandtl number the inclusion of thermal effects resulted in the addition of a 'nose'-shaped piece to the neutral stability curve at smaller wave-numbers. The resulting curve showed two local minima of the Reynolds number. In addition phase velocities in excess of the maximum flow velocity were found. Recent experiments by Polymeropoulos & Gebhart (1967) in air are in agreement with Nachtsheim's results.

The system to be studied here differs from those above in that a *vertical* temperature gradient is present. Due to an analogy between stratified and rotating fluids, the basic system is analogous to a laminar Ekman layer and, for unit Prandtl number, the stability problem is the same (Gill 1966, §4) as that of an Ekman layer to rolls aligned with the external flow. The neutral stability curve found by Lilly (1966) for the latter problem is qualitatively very similar to the one found by Nachtsheim for the uniform flux plate problem at a Prandtl number of 0·733. In the rotating fluid case disturbance energy can be acquired through the action of Coriolis forces and the associated instability can thus be called a Coriolis-driven instability.

Only two-dimensional disturbances are studied in this paper even though Squire's theorem does *not* apply, owing to the presence of the basic vertical temperature gradient. In systems where no such gradient exists Squire's theorem *is* valid (Nachtsheim 1963).

2. Equations and boundary conditions

A fluid of kinematic viscosity ν, thermal diffusivitity κ and coefficient of cubical expansion γ occupies the half space $x_* > 0$ bounded by a vertical wall $x_* = 0$. A uniform stable vertical temperature gradient G is imposed on the whole system and relative to this gradient the temperature of the wall is raised by a fixed amount ΔT above that of the fluid at large distances from the wall. This gives rise to horizontal temperature gradients and buoyancy-driven motion in a layer near the wall. The width of the layer is of order l and vertical velocities of order V are produced, where

$$l^2 = 2(\nu\kappa)^{\frac{1}{2}}/N,$$

$$V = \gamma g \Delta T/\sigma^{\frac{1}{2}}N,$$

where $N = (\gamma g G)^{\frac{1}{2}}$ is the Brunt–Väisälä frequency, $\sigma = \nu/\kappa$ is the Prandtl number and g is the acceleration due to gravity. The Reynolds number R of the flow is given by

$$R = \frac{Vl}{\nu} = \frac{\gamma g \Delta T l^3}{2\nu^2} = \frac{2^{\frac{1}{2}}\gamma g \Delta T}{5(\nu\kappa)^{\frac{1}{4}}N^{\frac{3}{2}}} = \frac{\Delta T}{\sigma G l}.$$

The second expression for R shows that it may also be interpreted as a Grashof number. The third expression for R is in terms of given quantities. The fourth expression shows that R is related to the slope of the isotherms.

Using l, V, and ΔT as units of length, velocity and temperature, one can define non-dimensional co-ordinates, x, z, where z increases vertically upwards, corresponding non-dimensional velocity components u, w, a non-dimensional time t and a non-dimensional temperature ϑ relative to the uniform vertical gradient. The continuity equation implies the existence of a stream function ψ such that

$$u = -\psi_z, \quad w = \psi_x$$

and the vorticity and heat equations are

$$R\frac{D}{Dt}\nabla^2\psi = 2\vartheta_x + \nabla^4\psi,$$

$$\sigma R\frac{D}{Dt}\vartheta + 2\psi_x = \nabla^2\vartheta,$$

where

$$\frac{D}{Dt} = \frac{\partial}{\partial t} - \psi_z\frac{\partial}{\partial x} + \psi_x\frac{\partial}{\partial z}.$$

The second term in the heat equation arises because of the definition of ϑ as a temperature *relative* to the uniform vertical gradient.

The solution (see Gill 1966, § 4) for the undisturbed state is

$$w = W(x) = e^{-x}\sin x,$$

$$\vartheta = \Theta(x) \equiv e^{-x}\cos x,$$

and we consider perturbation to the stream function and temperature of the respective forms

$$\mathscr{R}\{\phi(x)\,e^{i\alpha(z-ct)}\}$$

and

$$\mathscr{R}\{\theta(x)\,e^{i\alpha(z-ct)}\},$$

where α and c are constants. The linear stability equations obtained by substitution in the vorticity and heat equations, neglecting products of disturbance functions, are

$$\phi^{\mathrm{iv}} - 2\alpha^2\phi'' + \alpha^4\phi - i\alpha R[(W-c)(\phi''-\alpha^2\phi) - W''\phi] + 2\theta' = 0, \tag{2.1}$$

$$\theta'' - \alpha^2\theta - i\alpha\sigma R[(W-c)\theta - \Theta'\phi] - 2\phi' = 0. \tag{2.2}$$

These differ from the equations for a system without a vertical temperature gradient only through the presence of the last term in the second equation. The boundary conditions are

$$\phi = \phi' = \theta = 0 \quad \text{at} \quad x = 0 \tag{2.3}$$

and

$$\phi, \theta \to 0 \quad \text{as} \quad x \to \infty. \tag{2.4}$$

The three solutions that satisfy the latter condition behave like $\exp(-\lambda x)$ as $x \to \infty$, where λ is one of the three roots of

$$(\lambda^2-\alpha^2)(\lambda^2-\alpha^2+i\alpha Rc)(\lambda^2-\alpha^2+i\alpha\sigma Rc) + 4\lambda^2 = 0,$$

which has positive real part λ_r. We number the roots so that

$$\lambda_{1r} \leqslant \lambda_{2r} \leqslant \lambda_{3r}.$$

If any of these roots have real part small compared with unity, the corresponding solutions are likely to provide significant contributions to θ and ϕ at the terminal point $x = x_1$ of integration. For this reason, the outer boundary condition (2.4) was replaced by

$$\mathbf{M}\phi = \mathbf{M}\phi' = \mathbf{M}\theta = 0 \quad \text{at} \quad x = x_1, \tag{2.5}$$

where either (i) $\mathbf{M} = d/dx + \lambda_1$,

or (ii) $\mathbf{M} = d^2/dx^2 + (\lambda_1+\lambda_2)\,d/dx + \lambda_1\lambda_2$.

The first choice was found satisfactory for $0{\cdot}4 \leqslant \sigma \leqslant 2$, but it was necessary to use the second choice for other values of σ. The terminal point x_1 was usually between 6 and 10. If $x > 2\pi$, W, Θ and their derivatives are less than 0·2 % of their maximum values.

Integrals of the equations

The energy integral can be obtained from (2.1) by multiplying the complex conjugate $\bar{\phi}$ of ϕ, integrating from $x = 0$ to $x = \infty$ and taking the real part. The resulting equation (Nachtsheim 1963, p. 11) is

$$\alpha Rc_i E_M = -D_M + RM + B, \tag{2.6}$$

where

$$\left.\begin{aligned} E_M &= \int_0^\infty (|\phi'|^2 + |\alpha\phi|^2)\,dx, \\ D_M &= \int_0^\infty |\phi'' - \alpha^2\phi|^2\,dx, \\ M &= \alpha\int_0^\infty W'(\phi_i'\phi_r - \phi_r'\phi_i)\,dx, \\ B &= 2\int_0^\infty (\theta_r\phi_r' + \theta_i\phi_i')\,dx, \end{aligned}\right\} \tag{2.7}$$

and the suffixes r and i denote real and imaginary parts. $\alpha Rc_i E_M$ can be interpreted as the rate of change of disturbance kinetic energy, D_M as the rate of viscous dissipation, RM as the rate of transfer of kinetic energy from the mean flow to the disturbance and B as the rate of gain of disturbance kinetic energy through the action of buoyancy forces. A similar relation for temperature fluctuations can be obtained by multiplying (2.2) by $\tilde{\theta}$, integrating from $x = 0$ to $x = \infty$ and taking the real part. The resulting equation is

$$\alpha\sigma Rc_i E_T = -D_T + \sigma RH - B, \tag{2.8}$$

where

$$E_T = \int_0^\infty |\theta|^2 \, dx,$$

$$\left.\begin{aligned} D_T &= \int_0^\infty (|\theta'|^2 + |\alpha\theta|^2)\, dz \\ \text{and} \quad H &= \alpha \int_0^\infty \Theta'(\theta_i \phi_r - \theta_r \phi_i)\, dx. \end{aligned}\right\} \tag{2.9}$$

The term $-B$ appears in (2.8) only when a vertical temperature gradient is present. When there is such a gradient, $\alpha\sigma Rc_i E_T$ can be interpreted as the rate of gain of disturbance potential energy, D_M as the rate of thermal dissipation, σRH as the rate of extraction of disturbance potential energy from the basic temperature field and B as the rate of conversion of disturance potential energy into disturbance kinetic energy. Also (2.6) and (2.8) can be added to give an equation for the total disturbance energy

$$\alpha Rc_i(E_M + \sigma E_T) = -(D_M + D_T) + R(M + \sigma H). \tag{2.10}$$

Since E_M, E_T, D_M and D_T are positive definite, it follows that either M or H must be positive if disturbances are to grow. If M is positive, disturbance energy is gained from the basic *velocity* field while if H is positive, disturbance energy is gained from the basic *temperature* field.

We add two cautionary notes about the above equations. The first is that (2.10) can only be derived when there is a basic vertical temperature gradient, whereas Nachtsheim's results suggest that the stability characteristics are much the same when there is no such gradient. We therefore try to avoid interpreting results in terms that are only meaningful when a vertical temperature gradient exists. Secondly, we note that the above equations are derived on the basis of linear disturbance theory. To relate 'disturbance energy' to the energy of the whole system requires proper consideration of effects of second order in the disturbance velocity and temperature.

3. Neutral stability curves

The basic program was designed to find neutral stability curves, that is curves $R(\alpha, \sigma)$ on which the imaginary part β_i of $\beta = \alpha c$ is zero. The equations were integrated numerically using a Runge–Kutta marching procedure beginning at $x = 0$ where the conditions (2.3) and the normalization $\phi''(0) = 1$ were applied. For a given value of α, guessed values of R, β_r, $\phi''(0)$ and $\theta'(0)$ were used, and the

integration carried to $x = x_1$. After repeating with slightly different values of $\phi'''(0)$ and $\theta'(0)$, linear interpolation was used as the inner loop of an iterative process designed to find values such that $\mathbf{M}\phi'$ and $\mathbf{M}\theta$ vanished at $x = x_1$. This was contained in an outer loop which was used to find values of R, β, such that $\mathbf{M}\phi$ also vanished and (2.5) was satisfied. Alternatively R was kept fixed and appropriate values of α found. The latter scheme was used to find those parts of the neutral stability curves for which $d\alpha/dR$ was small. Tests were made

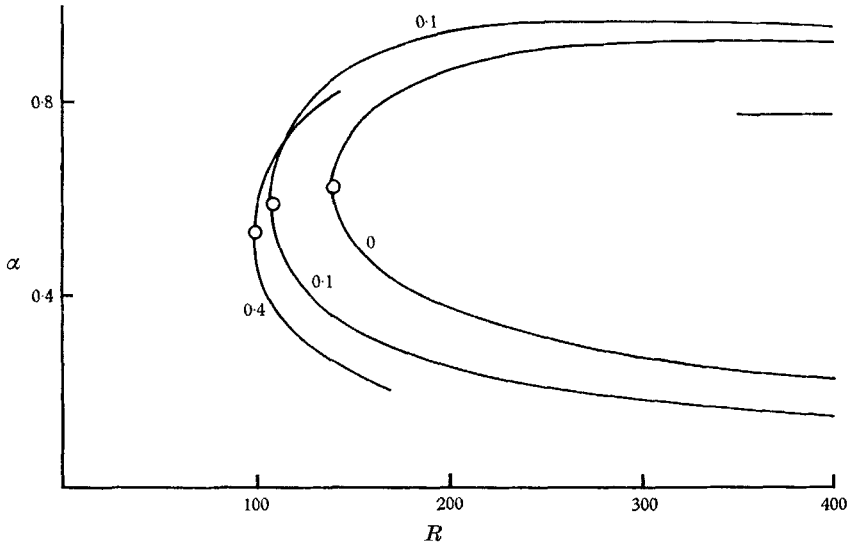

FIGURE 1. Neutral stability curves for Prandtl numbers $\sigma = 0$, 0·1 and 0·4. The circles indicate critical values and the line segment shows the large R asymptote deduced from the Rayleigh equation.

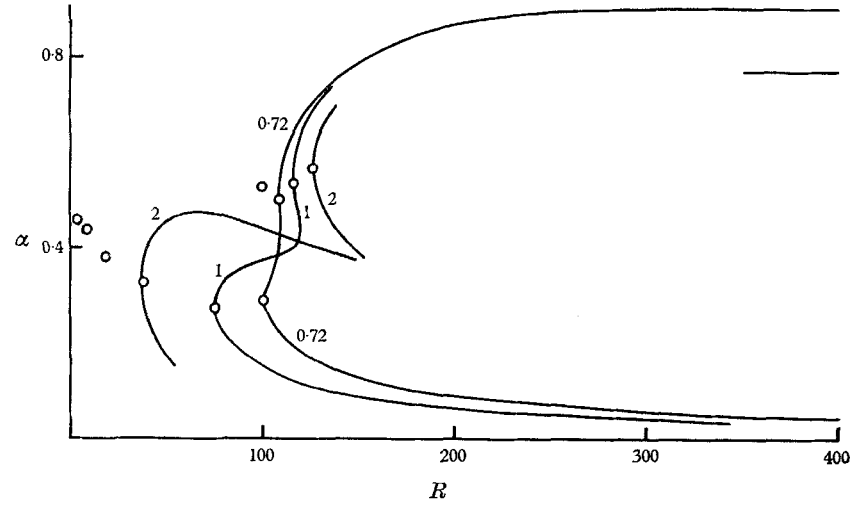

FIGURE 2. Neutral stability curves for Prandtl numbers $\sigma = 0{\cdot}72$, 1 and 2. The circles indicate critical values including those for $\sigma = 0{\cdot}4$, 4, 10 and 20. The line segment shows the large R asymptote deduced from the Rayleigh equation.

	σ	α	c	R	$\sigma^{\frac{1}{2}}R$	E_M	E_T	D_M	D_T	RM	σRH	B
(i)	0	0·620	0·164	141	—	0·138	0·142	0·423	0·156	0·580	0	−0·156
	0·1	0·588	0·172	109	—	0·200	0·075	0·491	0·110	0·585	0·017	−0·093
	0·4	0·526	0·191	100	—	0·237	0·380	0·532	0·631	0·519	0·645	0·013
	0·72	0·502	0·200	109	—	0·225	0·727	0·542	1·357	0·458	1·441	0·084
	1	0·539	0·194	117	—	0·181	0·768	0·503	1·678	0·434	1·748	0·070
	2	0·566	0·188	127	—	0·151	0·852	0·480	2·78	0·423	2·84	0·057
(ii)	0·72	0·289	0·281	101	85·9	0·74	1·55	1·00	2·49	0·39	3·10	0·61
	1	0·278	0·313	76·1	76·1	1·06	2·20	1·28	3·71	0·16	4·83	1·12
	2	0·326	0·347	37·9	53·6	1·46	2·94	1·70	5·54	−0·18	7·41	1·87
	4	0·381	0·375	19·1	38·3	1·73	2·95	2·03	6·03	−0·25	8·31	2·28
	10	0·436	0·409	8·50	26·9	1·94	2·41	2·20	5·34	−0·16	7·71	2·36
	20	0·458	0·432	4·94	22·1	2·02	1·99	2·20	4·68	−0·093	6·97	2·29
	50	0·465	0·456	2·62	18·5	2·19	1·66	2·17	4·10	−0·041	6·31	2·21
	100	0·463	0·471	1·70	17·0	2·32	1·52	2·17	3·94	−0·0215	6·13	2·19
	200	0·454	0·482	1·15	16·2	2·45	1·44	2·18	3·90	−0·0112	6·11	2·21
	400	0·445	0·491	0·79	15·9	2·57	1·41	2·20	3·95	−0·0059	6·18	2·24
	∞	0·417	0·512	0	15·0	2·81	1·40	2·20	3·72	0	5·92	2·20

TABLE 1. Critical values of R and the corresponding values of α, c and the integrals (2.7) and (2.9) of the appropriate eigenfunctions: (i) larger wave-number critical values; (ii) smaller wave-number critical values. The eigenfunctions are based on the normalization $\phi''(0) = 1$.

for dependence of the eigenvalues on the step length d and the terminal point x_1. Values were chosen to minimize the computing subject to the error in the magnitude of the eigenvalue being of the order of 0·1 %. Values of d between 0·12 and 0·20 were generally found adequate and values of x_1 between 6 and 10.

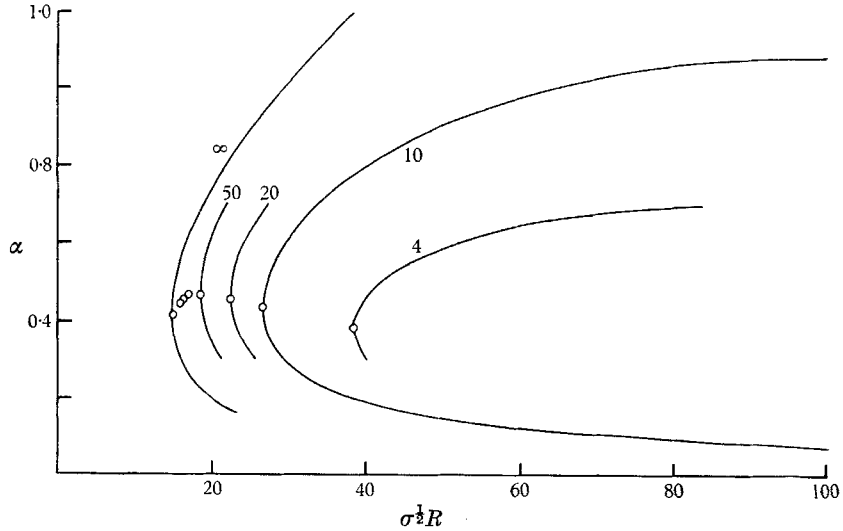

FIGURE 3. Neutral stability curves for Prandtl numbers $\sigma = 4$, 10, 20, 50 and ∞. The circles indicate critical values including those for $\sigma = 100$, 200 and 400.

The aim of the program was to find neutral stability curves, or at least portions of them, for the whole range of Prandtl numbers. Calculations were in fact made for the fourteen different values of σ listed in table 1, including the limiting values $\sigma = 0$ and $\sigma = \infty$ and the value $\sigma = 1$ for which there is a direct analogy with the stability problem for a laminar Ekman layer. A selection of the calculated curves is shown in the first three figures. The curves show some rather interesting changes as σ increases through the values for which computations were done. First there is the development of the 'nose'-shaped piece on the curves at $\sigma = 0{\cdot}72$ and $\sigma = 1$. These nose-shaped pieces are very similar to the one found by Nachtsheim (1963) for the flux-plate problem for $\sigma = 0{\cdot}733$ and shown by him to disappear when buoyancy effects on the instability were ignored. The same feature is implicit in Lilly's (1966) results for the laminar Ekman layer, that is the neutral stability curves have a nose-shaped piece which disappears when Coriolis effects on the instability are ignored. Hence the 'nose'-shaped part of the curve of lower wave numbers can be said to represent the difference between the full stability problem and the Orr–Sommerfeld problem for the same velocity profile.

The second interesting development is the branching off of the nose-shaped piece, first apparent at $\sigma = 2$, so that there are then two unstable modes. In contradistinction, Lilly never found more than one unstable mode for $\sigma = 1$ even though his method involved the calculation of eigenvalues for several modes. To check that there are indeed two unstable modes for $\sigma = 2$, two curves of αc_i against α were calculated for $R = 150$ as follows. One curve was found by

starting near the neutral curve at $\alpha = 0{\cdot}7$ and following the changes in αc_i as α was decreased in small steps. The other curve was found by starting near the neutral curve at $\alpha = 0{\cdot}04$ and increasing α in small steps. The two resulting curves are shown in figure 4 by solid lines. For comparison the results of a similar calculation for $\sigma = 1$ is shown by the broken line.

A third interesting feature of the neutral stability curves is the behaviour as σ tends to infinity. For $\sigma > 2$ only the curve with the lowest critical Reynolds number was calculated and it was found that as $\sigma \to \infty$, the critical Reynolds number approached zero like $\sigma^{-\frac{1}{2}}$. The large σ limit will be discussed in detail in §5.

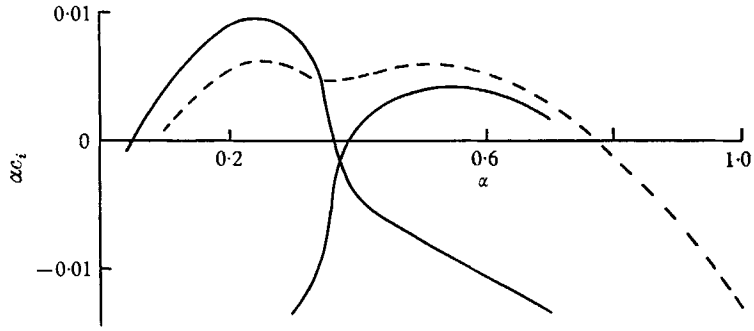

FIGURE 4. The growth rate αc_i as a function of wave-number α at a Reynolds number of 150. For a Prandtl number of 2 (solid lines) two different modes are represented. The broken line shows the corresponding mode for a Prandtl number of 1.

Before going further, mention should be made of a comparison that was made between the results for $\sigma = 1$ and Lilly's (1966) results for the analogue problem. For direct comparison with the results for $\epsilon = 0$ shown in his figures 6, 7 and 8, the variation of growth rate αc_i with α was calculated for Reynolds numbers of 110, 150 and 500. Agreement was not perfect, the differences in αc_i usually being about 0·001 with a few larger differences for $R = 500$. We feel that this indicates errors of this order in Lilly's results as we consider our errors in αc_i to be less than 10^{-4}. The difference is possibly due to Lilly's use of a coarser mesh. We used 60 intervals of 0·15 whereas Lilly (with a different method) used 35 intervals of $(35\alpha)^{-\frac{1}{2}}$, that is, intervals as great as 0·53 for $\alpha = 0{\cdot}1$.

The critical Reynolds numbers, defined as minima of $R(\alpha)$, that were found are listed in table 1. These seem to fall naturally into two groups and are so divided in the table. For $\sigma = 0{\cdot}72$ and $\sigma = 1$ it is evident that the critical values in the second group owe their existence to the 'nose'-shaped piece on the neutral stability curves and hence to the effects of buoyancy on the instability. The division of critical points into two groups is also evident in figure 5 where the waves speed c is shown as a function of wave-number α. For $\sigma \leqslant 2$, the changes of c with σ are most pronounced at the smaller wave-numbers. For instance, the curves for $\sigma = 0{\cdot}72$ and $\sigma = 1$ are practically coincident for $\alpha > 0{\cdot}4$, but quite distinct for the smaller wave-numbers. At $\sigma = 2$, where the neutral stability curve splits the $c = \alpha$ curve is rather interesting. The part which corresponds to the upper curve for $\alpha > 0{\cdot}4$ is not drawn as it is almost coincident with the curves for

$\sigma = 0{\cdot}72$ and $\sigma = 1$. The part that is drawn corresponds to the lower curve. Its rather exceptional shape is presumably associated with the splitting into two of the neutral stability curve.

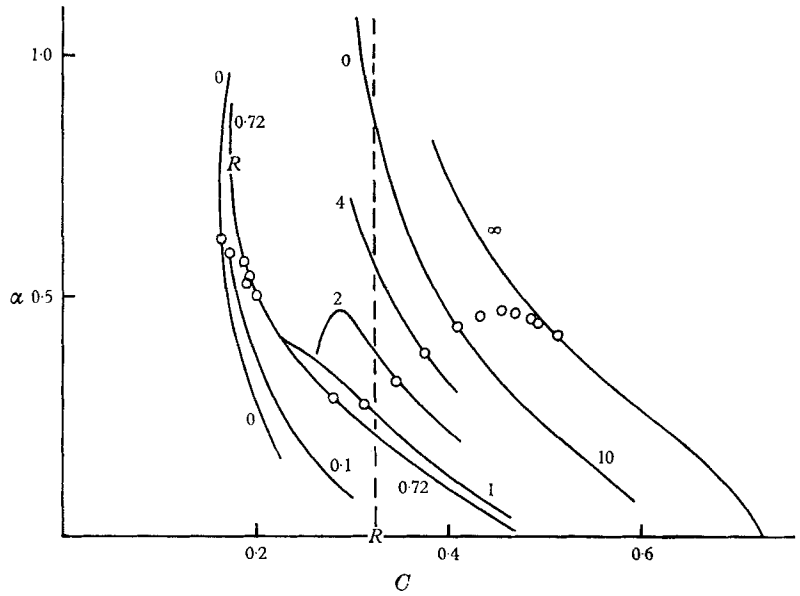

FIGURE 5. The wave speed c of neutral disturbances as a function of wave-number α and Prandtl number. The small circles indicate the critical values listed in table 1. The two points R correspond to solutions of the Rayleigh equation, and the broken line corresponds to $c = W_{\max}$.

It will be noticed that c is often greater than the maximum value 0·3224 of W. If effects of buoyancy on the disturbance were ignored, c would, of course, be constrained to lie below the maximum value of W, so this result may be regarded as a buoyancy effect. Nachtsheim drew attention to the fact that c is greater than the maximum velocity in other problems involving gravitational forces, such as in the case of flow down an inclined plane (Benjamin 1957).

Another study that was made of the neutral stability curves was aimed at detecting the limiting behaviour for large Reynolds numbers. The upper branches of the neutral curves for $\sigma = 0$, 0·72 and 1 were followed to fairly large values of the Reynolds number (614, 533 and 500 respectively) but in none of these cases was there any indication that a limit was being approached. In each case, both α and c had attained their maximum values and were slowly decreasing as R increased at the point where the calculation was terminated. It is to be expected (see Gregory, Stuart & Walker 1955; Szewczyk 1962; and Barcilon 1965 for relevant comments) that as $\alpha R \to \infty$, the solution will tend to a solution of the Rayleigh equation (6.1). This equation is discussed in §6. The limiting value, 0·77, of α corresponding to the solution of the Rayleigh equation is shown in figures 1 and 2 and the limiting values 0·1778 and 0·3224 of c are marked R in figure 5. Evidently the calculation of the neutral stability curves would need to be taken

to much larger values of the Reynolds number before it could be seen whether values corresponding to solutions of the Rayleigh equations are approached.

The lower branches of the neutral stability curves for $\sigma = 0{\cdot}72$, 1 and 10 were also carried to fairly large values of R. In these cases, plots of log α against log R indicated that αR tends to fixed values as $R \to \infty$, the values being 17·3, 13·3 and 2·33 respectively for the three above values of σ. Thus solutions do not tend to those of the Rayleigh equations but rather to a boundary-layer type of approximation to the stability equations, obtained by putting $\alpha R =$ constant, $\alpha = 0$ in (2.1) and (2.2). Similar plots of log α against log R for the lower branches of the neutral stability curves for $\sigma = 0{\cdot}1$ and $\sigma = 0$ did not show the same behaviour. One suspects that in the case of $\sigma = 0{\cdot}1$ this was due to the calculation being stopped at too small a value of R. For the case $\sigma = 0$ it is possible that $\alpha R \to \infty$ as $R \to \infty$ on the lower branch and that the solution tends to a solution of the Rayleigh equation. The corresponding limiting value of c is shown by a letter R in figure 5 and it is possible that the $\sigma = 0$ curve approaches this as $\alpha \to 0$.

4. Eigenfunctions

The eigenfunctions ϕ and θ were calculated at all the critical values (α, R) listed in table 1 and the integrals (2.7) and (2.9) calculated. Figures 6–13 show a selection of the functions calculated and the integrals are listed in table 1.

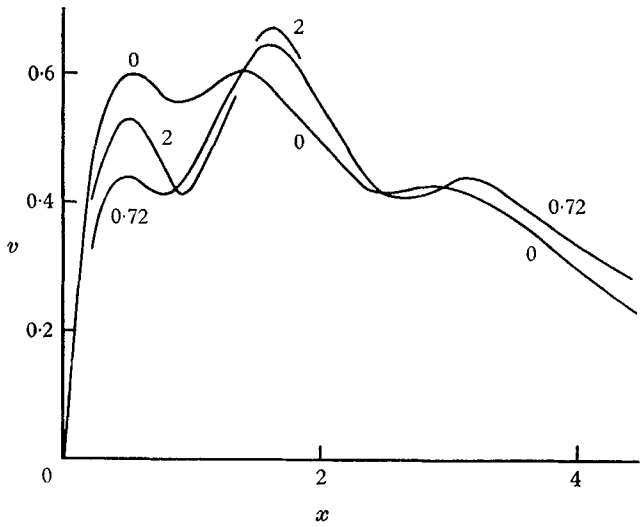

FIGURE 6. Root-mean-square disturbance velocity, v, as a function of x at larger wave-number critical values for Prandtl numbers $\sigma = 0$, 0·72 and 2. The ordinate is chosen in each case so that the integral across the layer of $v^2 = \frac{1}{2}\{|\phi'|^2 + |\alpha\phi|^2\}$ is unity.

Let us first discuss the integrals. These were calculated independently of the relations (2.6) and (2.8) which serve as a check on their accuracy. The values in table 1 are divided into two groups and it is evident that the energy balances (2.6) in one group are quite different from those in the other. In the first group the rate B of working of buoyancy forces is small compared with the rate RM of transfer

of kinetic energy from the mean flow to the disturbance. In the second group the reverse is true. For this reason it appears appropriate to associate the first group of values with a 'mechanically-driven instability' and the second group with a 'buoyancy-driven instability'. Other evidence for this identification stems

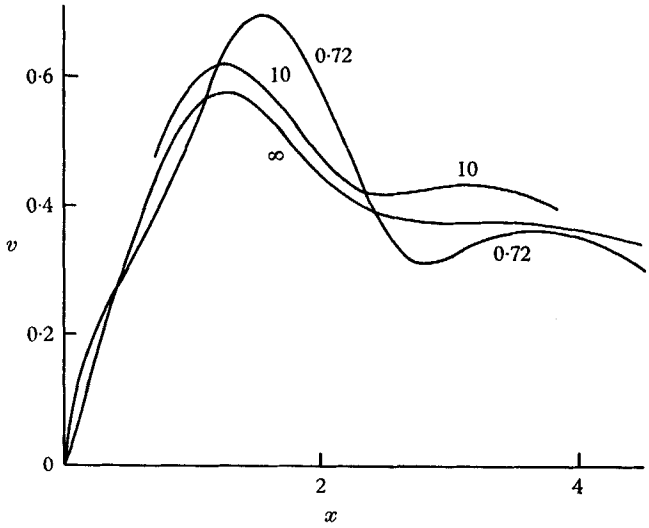

FIGURE 7. Root-mean-square disturbance velocity v, as a function of x at smaller wave-number critical values for Prandtl numbers $\sigma = 0{\cdot}72$, 10 and ∞. The ordinate is chosen in each case so that the integral across the layer $v^2 = \frac{1}{2}\{|\phi'|^2 + |\alpha\phi|^2\}$ is unity.

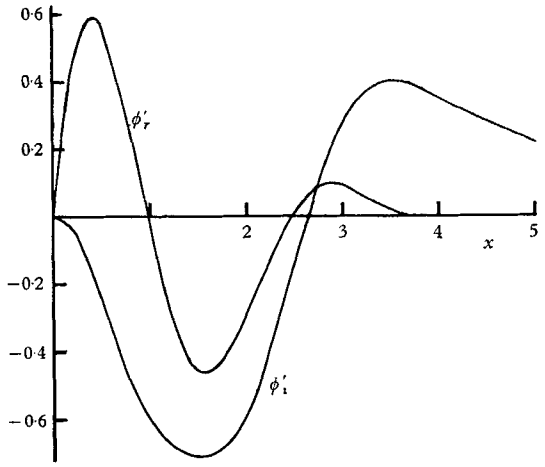

FIGURE 8. Real and imaginary parts of $\phi'(x)$ at the larger wave-number critical value for the Prandtl number $\sigma = 0{\cdot}72$. The normalization is the same as in figure 6.

from the results of Nachtsheim (1963) and Lilly (1966) which show that for Prandtl numbers around unity, the upper wave-number critical values are not changed very much when buoyancy effects are neglected whereas the lower wave-number critical values disappear.

Details of disturbance velocity and temperature profiles are given in figures

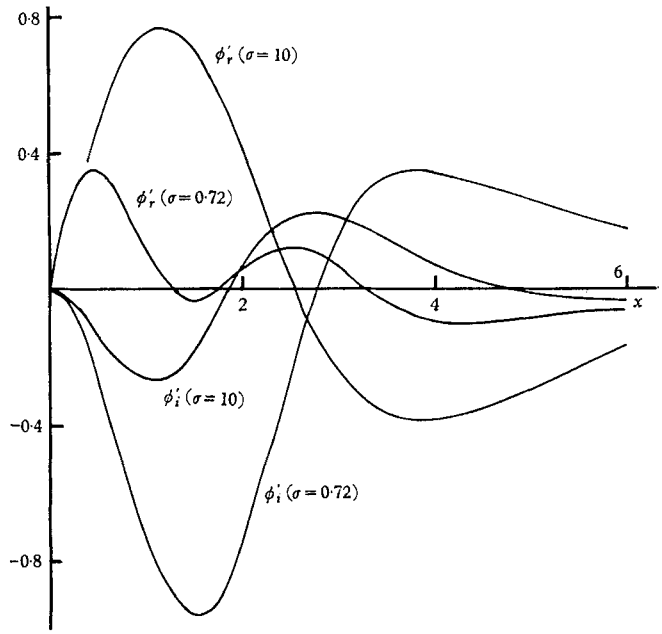

FIGURE 9. Real and imaginary parts of $\phi'(x)$ at the small wave-number critical value for Prandtl numbers, $\sigma = 0{\cdot}72$ and 10. The normalization is the same as in figure 7.

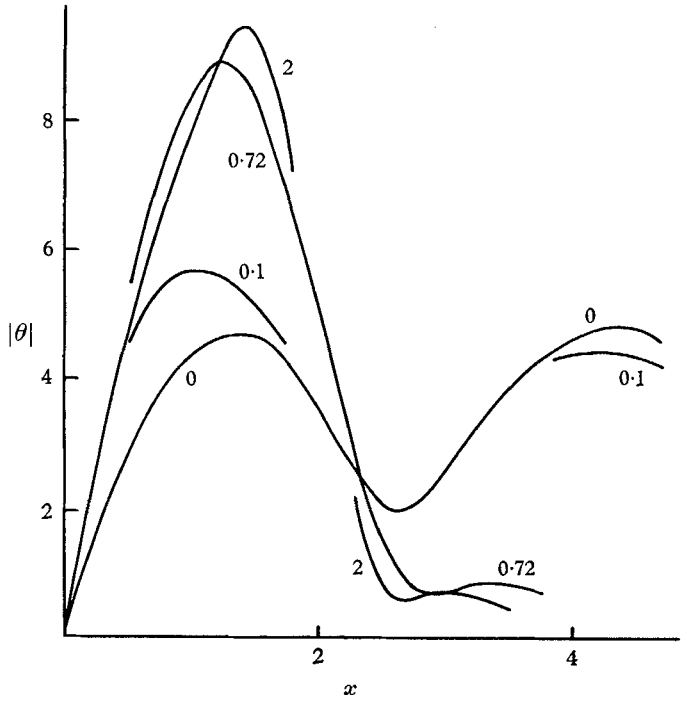

FIGURE 10. Amplitude, $|\theta|$, of disturbance temperature as a function of x at larger wave-number critical values for Prandtl numbers $\sigma = 0$, 0·1, 0·72 and 2. The ordinate is chosen in each case so that the integral across the layer of $|\theta|^2$ is unity. This is *not* the same normalization as in figure 6.

6–11. It will be noted that although temperature fluctuations are only significant within the boundary layer, defined by $x < 2$ say, velocity fluctuations are felt over a much wider region, say $x < 4$. Now compare figures 6 and 7. The velocity curves

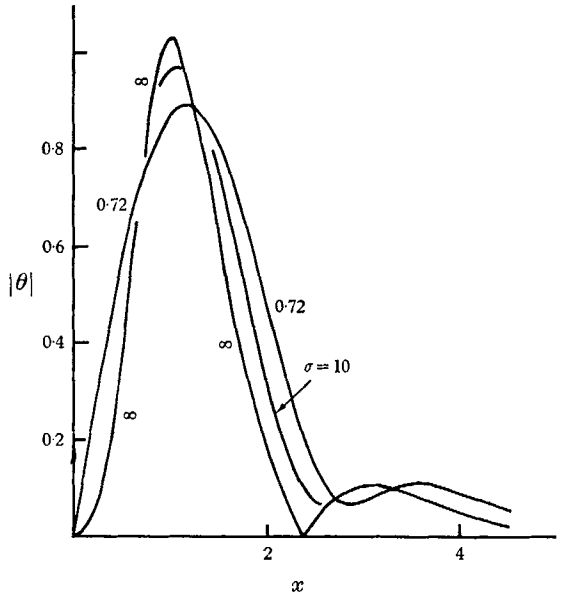

FIGURE 11. Amplitude, $|\theta|$, of disturbance temperature as a function of x at smaller wave-number critical values for Prandtl numbers $\sigma = 0{\cdot}72$, 10 and ∞. The ordinate is chosen in each case so that the integral across the layer of $|\theta|^2$ is unity. This is *not* the same normalization as in figure 7.

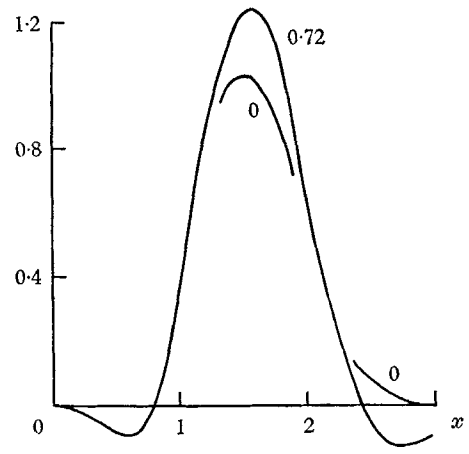

FIGURE 12

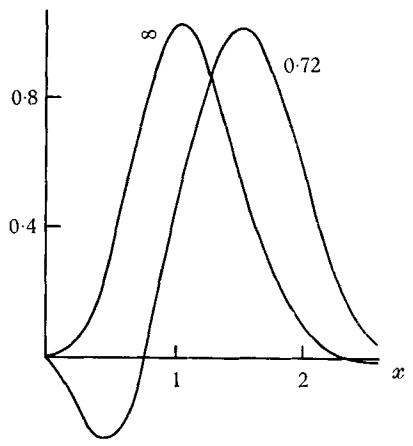

FIGURE 13

FIGURE 12. The rate $\alpha W'(\phi_r\phi_i' - \phi_r'\phi_i)$ at which work is done by the Reynolds stresses as a function of x at larger wave-number critical values for Prandtl numbers $\sigma = 0$ and $0{\cdot}72$. The ordinate is chosen so that the area under each curve is unity.

FIGURE 13. The rate $2(\theta_r\phi_r' + \theta_i\phi_i')$ at which work is done by buoyancy forces as a function of x at smaller wave-number critical values for Prandtl numbers $\sigma = 0{\cdot}72$ and ∞. The ordinate is chosen so that the area under the curve is unity.

in figure 6, which correspond to the mechanically driven instability, show two prominent peaks, while those in figure 7 show only one. This is presumably associated with the fact that, in the former case, there are two distinct critical points, that is, points where $W = c_r$. In the latter case either the two critical points are relatively close together or $c_r > W$ and there are no critical points.

On the whole the curves for either group vary remarkably little with σ but there are some exceptions. For instance, figure 9 shows that the curves for ϕ_r', ϕ_i' do change significantly with σ even though the corresponding curves for v may not. Also figure 10 shows that the curves are rather different at low Prandtl numbers. This is because, for given ϕ, the type of θ distribution depends on whether $\alpha\sigma R$ is large or small, as can be seen from (2.2). It turns out that $\alpha\sigma R$ is 'large' unless σ is quite small.

Figures 12 and 13 show the terms which correspond to the main source of disturbance kinetic energy for the case in question. They are simple curves with only one prominent maximum in each case.

5. The large Prandtl number limit

The instability due to the action of buoyancy forces is a rather interesting one, the mechanism being quite different from that studied in connexion with the Orr–Sommerfeld equation. This mechanism dominates at large Prandtl numbers for then the advection of vorticity which is necessary for an Orr–Sommerfeld type of instability is relatively unimportant. Assuming that some simplification in the equations occurs in the limit, it seems possible that more about the buoyancy-driven instability can be learnt by examining this limit.

Before neutral stability curves were calculated for $\sigma > 10$, it was thought that the corresponding curve for $\sigma = \infty$ could be found by formally placing $R = 0$ in (2.1) and (2.2) and assuming a finite value of the Péclet number σR. No neutrally stable solutions were found, however, under this assumption so it was decided to calculate αc_i as a function of α and σR (with $R = 0$). This was done for $\sigma R = 100$, $\alpha = 0{\cdot}3$ to $0{\cdot}6$; for $\alpha = 0{\cdot}3$, $\sigma R = 100$ to 250; and for $\alpha = 0{\cdot}6$, $\sigma R = 100$ to 150. The values of αc_i obtained were negative and it appeared that $\alpha\sigma R c_i$ was a function of α only. The minimum value of $|\alpha\sigma R c_i|$ occurred at about $\alpha = 0{\cdot}56$ being $3{\cdot}9$.

If any instability did occur for $R = 0$, $\sigma R \neq 0$, one would at least expect instability when σR is large. In the formal limit, $R \to 0$, $\sigma R \to \infty$, (2.1) and (2.2) become the fourth-order system

$$\left.\begin{aligned} \phi^{\mathrm{iv}} - 2\alpha^2\phi'' + \alpha^4\phi + 2\theta' &= 0, \\ (W-c)\,\theta - \Theta'\phi &= 0, \end{aligned}\right\} \tag{5.1}$$

where ϕ, ϕ' vanish at $x = 0$ and $x = \infty$. Solutions of these equations were examined numerically for α between $0{\cdot}16$ and $0{\cdot}82$ and found, rather surprisingly, to be *neutrally* stable, i.e. the eigenvalue c was found to be real for each value of α.

In order to investigate the limit $\sigma \to \infty$ for the full sixth-order system, the neutral stability curves for $\sigma = 10$ to 400 were calculated and examined. These

indicated that as $\sigma \to \infty$, values of $\sigma^{\frac{1}{2}}R = S$ on the neutral curve remain finite. It was then noted that under the formal limit $\sigma \to \infty$, S fixed, $\phi \to \phi_0$, $c \to c_0$, (2.1) and (2.2) reduce to (5.1), that is ϕ_0 and c_0 satisfy

$$L\phi_0 \equiv \phi_0^{\mathrm{iv}} - 2\alpha^2\phi_0'' + \alpha^4\phi_0 + \left(\frac{2\Theta'\phi_0}{W-c_0}\right)' = 0. \tag{5.2}$$

Even though this equation is only of fourth order, *all* the boundary conditions of the full sixth-order equation are satisfied if we set $\phi_0 = \phi_0' = 0$ at $x = 0$ and $x = \infty$. Values of $c_0(\alpha)$ were computed and these are shown in figure 5 as the curve labelled $\sigma = \infty$. All computed values of c_0 were real and greater than the maximum value of W. Since the values of c_0 for α between 0·6 and 0·82 fit the relation

$$c_0 - w_{\max} = 0{\cdot}042\alpha^{-2}$$

quite well, it seems quite likely that $c_0 > w_{\max}$ for *all* α. We did not, however, calculate solutions for large α as there seems little practical motivation for doing so.

To find the growth rate αc_i and the values of S on the neutral curve, it is necessary to consider terms of order $\sigma^{-\frac{1}{2}}$. If we put

$$\left.\begin{aligned} \phi &= \phi_0 + i\sigma^{-\frac{1}{2}}\phi_1, \\ c &= c_0 + i\sigma^{-\frac{1}{2}}c_1, \end{aligned}\right\} \tag{5.3}$$

in (2.1) and (2.2), then the formal limit $\sigma \to \infty$ leads to an equation for ϕ_1 and c_1 of the form

$$L\phi_1 = f, \tag{5.4}$$

where

$$\begin{aligned} f &= \alpha S X - Y/\alpha S - c_1 Z, \\ X &= (W-c_0)(\phi_0'' - \alpha^2\phi_0) - W''\phi_0, \\ Y &= -2[(\theta_0'' - \alpha^2\theta_0 - 2\phi_0')/(W-c_0)]', \\ Z &= 2[\theta_0/(W-c_0)]'. \end{aligned} \tag{5.5}$$

The appropriate boundary conditions are $\phi_1 = \phi_1' = 0$ at $x = 0, \infty$. These imply that θ_1 is finite at $x = 0$ so that a correction to θ_1 must be made in order to satisfy the boundary conditions of the full sixth-order equation. Examination of (2.1) and (2.2) shows, however, that the appropriate correction is significant only in a boundary layer against the wall of thickness $\sigma^{-\frac{1}{4}}$ and that ϕ_1 and c_1 are, at zero order, solutions of (5.4).

In order for (5.4) to have a solution it is necessary that

$$\int_0^\infty f\chi\,dx = \int_0^\infty \chi L\phi_1\,dx = \int_0^\infty \phi_1 L^*\chi\,dx = 0, \tag{5.6}$$

where χ is a solution of the adjoint problem

$$L^*\chi \equiv \chi^{\mathrm{iv}} - 2\alpha^2\chi'' + \alpha^4\chi - \frac{2\Theta'\chi'}{W-c_0} = 0, \tag{5.7}$$

with $\chi = \chi' = 0$ at $x = 0, \infty$. Substituting (5.5) in (5.6) gives

$$\alpha c_1 = a(\alpha)\,S - b(\alpha)/S, \tag{5.8}$$

where

$$\left.\begin{aligned} a(\alpha) &= \alpha^2 \int_0^\infty X\chi\,dx \Big/ \int_0^\infty Z\chi\,dx, \\ b(\alpha) &= \int_0^\infty Y\chi\,dx \Big/ \int_0^\infty Z\chi\,dx. \end{aligned}\right\} \tag{5.9}$$

Solutions χ of the adjoint equation (5.7) were computed and the integrals in (5.9) evaluated. a and b were found to be positive. Knowledge of $a(\alpha)$ and $b(\alpha)$ yields not only the $\sigma = \infty$ neutral stability curve shown in figure 3 but also the growth rate $\alpha\sigma^{-\frac{1}{2}}c_1$ as a function of α and S. Contours of constant αc_1 are drawn in figure 14. In the limit $R \to 0$, σR fixed, the first term on the right-hand side of (5.8) vanishes showing that $\alpha\sigma Rc_i$ is a function of α only as found in the calculation mentioned above. The minimum value of $(\alpha\sigma Rc_i)$ was found to be 4·0 at $\alpha = 0{\cdot}53$. These figures are not quite the same as those found by the previous method but then the previous calculation included the effects of higher-order terms so a small discrepancy is to be expected. For large S, $\alpha c_i/R$ is a function of α only having a maximum value of 0·019 when $\alpha = 0{\cdot}37$.

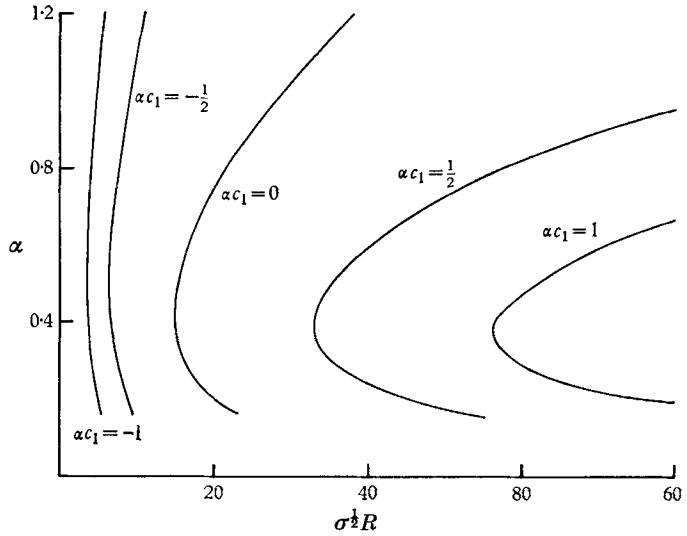

FIGURE 14. Contours of constant growth rate $\alpha c_i = \sigma^{-\frac{1}{2}}\alpha c_1$ in the limit as the Prandtl number σ tends to infinity. Note that αc_i is of order $\sigma^{-\frac{1}{2}}$.

The zero-order neutrally stable motion may be described as follows. For the values of α for which calculations were made, c is greater than the maximum value of W so that relative to an observer moving with velocity c, the stream is moving backwards. If the fluid in the boundary layer is moving upwards, the observer would see fluid particles moving downwards and executing small sinusoidal oscillations about a vertical line. The amplitude η of the oscillations is given by

$$\eta = \frac{\phi}{W - c_0} = \frac{\theta}{\Theta'}. \tag{5.10}$$

At points of maximum horizontal displacement, the horizontal velocity is zero while the temperature perturbation is a maximum. Thus, the horizontal velocity and temperature perturbation are out of phase so that there is no net horizontal heat flux and no tendency to increase the level of temperature fluctuations. To zero order in $\sigma^{-\frac{1}{2}}$, the disturbance energy equation (2.6) shows that the rate B of gain of disturbance kinetic energy through buoyancy forces is equal to

the rate D_M of viscous dissipation, that is all the energy produced by buoyancy effects is dissipated. Substituting from (5.10) into (2.7) and using the expressions for W and Θ, it can be shown that

$$B = 2\int_0^\infty (c_0 e^x \sin x - 1)\,\eta^2 e^{-2x}\,dx$$

and assuming contributions to the integral for $x > \pi$ are small, it is clear that, since B must be positive, c cannot be too small.

The first-order effects are of two different types. Those represented by the second term on the right-hand side of (5.8) correspond to diffusion effects and the effect of a stable gradient. These effects are stabilizing and give a negative contribution to c_i proportional to $(\sigma R)^{-1}$. The other first-order effect, represented by the first term on the right-hand side of (5.8) is advection of vorticity. This effect turns out to be destabilizing and gives a positive contribution to c_i proportional to R. In some ways, this is reminiscent of the behaviour of a fluid flowing down an inclined plane (Benjamin 1957): if αR is zero the flow is neutrally stable but first-order vorticity-advection effects lead to an instability with growth rate proportional to αR. Another similarity with the present problem pointed out by Nachtsheim (1963), is that the phase speed of the disturbance is greater than the maximum flow velocity. Although the flow may be rendered unstable through advection of vorticity, it does not follow that the instability is caused by transfer of energy from the mean flow. The expansion and the definition (2.7) imply that the rate RM of transfer of energy from the mean flow is of order σ^{-1}. Table 1 indicates that σRM tends to a negative value, $-2{\cdot}3$, as $\sigma \to \infty$, so that energy is being transferred *to* the mean flow from the disturbance. Thus the destabilizing effect must be due, in some way, to an increased effectiveness of the buoyancy force.

Because instability is produced by a first-order effect, the growth rate of the disturbance is very small, being of order $\sigma^{-\frac{1}{2}}$ when S is of order unity and of order R if S is large. Thus it will take a long time for an instability of this type to become evident. It is also implied that other small effects, such as finite amplitude effects, could well influence the stability in a laboratory situation.

One motivation for studying the large-σ limit was in order to obtain a simplified system of equations which might shed some light on the buoyancy-driven instability. Lilly (1966, §4) in his study of the stability of laminar Ekman layer suggested a 'simplified' theory of the analogous Coriolis instability, so it is of interest to try the corresponding 'approximations' in the present problem with σ not necessarily large. However, if this is done, it turns out that the predicted critical Reynolds number is independent of Prandtl number, so the theory is of doubtful value in the present context.

6. The Rayleigh equation

Under the formal limit $\alpha R \to \infty$, (2.1) reduces to the Rayleigh equation

$$(W - c)(\phi'' - \alpha^2\phi) - W''\phi = 0. \tag{6.1}$$

Thus there may be expected to be eigenvalues of the full equations (2.1) and (2.2)

which tend to those of the Rayleigh equation as $\alpha R \to \infty$. Because of this possibility, eigenvalues and eigenfunctions of (6.1), together with the boundary conditions

$$\left.\begin{aligned} \phi &= 0 \quad \text{at} \quad x = 0, \\ \phi &\to 0 \quad \text{as} \quad x \to \infty \end{aligned}\right\} \tag{6.2}$$

were found by direct numerical computation. The path of integration in the complex x-plane was chosen either to be the real part $x \geqslant 0$ of the real axis, or alternatively, the path given by

$$x = t - \beta i t W'(t), \tag{6.3}$$

with t real and positive and β a positive constant. The latter path was used especially when c_i was small in order to avoid the singularities and was chosen to pass the two singularities on the appropriate side (Lin 1955, chapter 8). The values

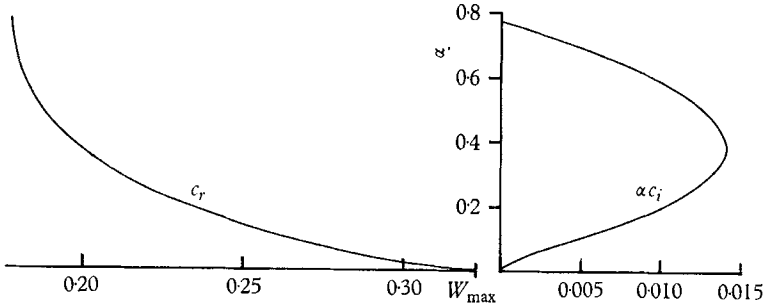

FIGURE 15. Wave speed c_r and growth rate αc_i as functions of α for solutions of the Rayleigh equation.

of c_r and c_i obtained are shown in figure 15. The maximum growth rate αc_i is 0·014 at $\alpha = 0{\cdot}39$. The distribution of disturbance velocity amplitude, v with x, is shown in figure 16 for a few values of α. The curve for $\alpha = 0$ is deduced from the theory below. The curve for $\alpha = 0{\cdot}4$ corresponding to a growth rate near the maximum value is quite similar to the curve shown in figure 6 for $\sigma = 0$. The latter curve corresponds to a solution of the full equations at a critical value of R.

As $\alpha \to 0$, c tends to the maximum value, 0·3224, of W and the two critical points come together. This eigenvalue is of a type discussed by Drazin & Howard (1962, § 6) although the details are a little different. In terms of the amplitude η defined (cf. 5.10) by

$$\eta = \phi/(W - c),$$

the Rayleigh equation is

$$[(W-c)^2\eta']' = \alpha^2(W-c)^2\eta. \tag{6.4}$$

For small α and finite x, the solution for which $\eta' + \alpha\eta$ vanishes at $x = \infty$ can be expanded as a series

$$\eta = 1 - \alpha\left\{x - \int_\infty^x \left[1 - \left(\frac{c}{W-c}\right)^2\right] dx\right\} + \ldots, \tag{6.5}$$

a particular normalization having been chosen.

Similarly, the solution vanishing at $x = 0$ can be expanded as a series

$$\eta = \delta\left\{\int_0^x \frac{dx}{(W-c)^2} + \ldots\right\}, \tag{6.6}$$

where δ is a constant. In view of the boundary conditions (6.2), solutions (6.5) and (6.6) must be different representations of the same solution.

Comparison of the two expressions for $(W-c)^2\eta'$ shows that

$$\delta = -\alpha c^2 + O(\alpha^2) \tag{6.7}$$

so that in the limit as $\alpha \to 0$,

$$\left.\begin{aligned} \eta &\to 1, \quad \phi \to W - W_m \quad \text{for} \quad x > x_m, \\ \eta &\to 0, \quad \phi \to 0 \qquad\quad \text{for} \quad x < x_m, \end{aligned}\right\} \tag{6.8}$$

where the suffix m denotes values at the point where W is a maximum. The curve for $\alpha = 0$ drawn in figure 16 is the one obtained from (6.8).

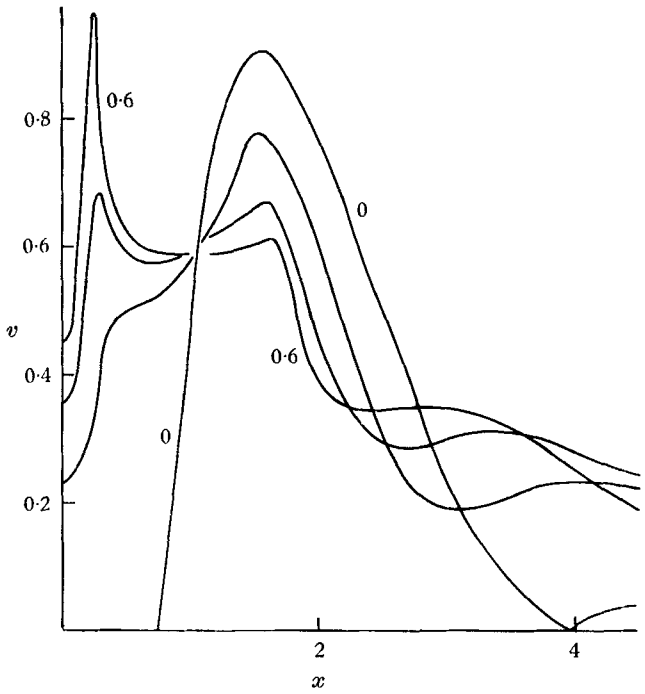

FIGURE 16. Root-mean-square disturbance velocity, v, as a function of x, corresponding to solutions of the Rayleigh equation for wave-numbers $\alpha = 0$, 0·2, 0·4 and 0·6. The ordinate is chosen in each case so that the integral across the layer of $v^2 = |\phi'|^2 + |\alpha\phi|^2$ is unity.

To find expressions for $c - W_m$, the solution must be examined in greater detail. Equating the two expressions (6.5) and (6.6) for η and noting the order of higher terms, one obtains the equality

$$1 + O(\alpha) = \alpha \int_0^\infty \left[1 - \left(\frac{c}{W-c}\right)^2\right] dx. \tag{6.9}$$

The contributions to the integral on the right-hand side which are large come from the neighbourhood of $x = x_m$ and may be inferred from the expression (6.15) of Drazin & Howard's paper which gives the local behaviour of the integral. Defining b by

$$c = W_m + \tfrac{1}{2} W_m'' b^2$$

and using the expression referred to, (6.9) becomes

$$1+O(\alpha) = \frac{-2\pi\alpha i}{b^3}\left(\frac{W_m}{-W_m''}\right)^2 (1+qb^2+O(b^4)),$$

where

$$q = \frac{W_m''}{W_m}+\frac{1}{8}\frac{W_m^{\mathrm{iv}}}{W_m''}-\frac{5}{24}\left(\frac{W_m'''}{W_m''}\right)^2.$$

Solving for b^2 and taking care to choose the correct root, one obtains

$$b^2 = \mu\alpha^{\frac{2}{3}}(1+\tfrac{2}{3}q\mu\alpha^{\frac{2}{3}}+O(\alpha)),$$

where

$$\mu = (2\pi)^{\frac{2}{3}}\left(\frac{W_m}{-W_m''}\right)^{\frac{4}{3}} e^{-\frac{1}{3}\pi i}.$$

Substituting the values of the derivatives of W_m one then obtains

$$c = W_m[1+(\tfrac{1}{2}\pi\alpha)^{\frac{2}{3}}\, e^{\frac{2}{3}\pi i}+\tfrac{31}{18}(\tfrac{1}{2}\pi\alpha)^{\frac{4}{3}}\, e^{-\frac{2}{3}\pi i}+O(\alpha^{\frac{5}{3}})].$$

This formula was checked against the computed results for $\alpha = 0{\cdot}02$ and $\alpha = 0{\cdot}04$. To the order shown, the above expression for $c - W_m$ was found to be correct to about 2 % at $\alpha = 0{\cdot}02$ and 5 % at $\alpha = 0{\cdot}04$.

7. Stability of convection in a vertical slot

It was noted in the introduction that the boundary layer under study is very much like that found at large Rayleigh numbers in a vertical slot (Elder 1965*a*; Gill 1966). Thus the above results may be expected to give some information about the stability of convection in a slot. If the slot has height H, width L and a temperature difference ΔT imposed between the two vertical side walls, there are three parameters which describe the system: the Rayleigh number $A = \gamma g \Delta T L^3/\kappa\nu$, the aspect ratio $h = H/L$ and the Prandtl number $\sigma = \nu/\kappa$. It is required that h be large enough for the flow to be approximately unidirectional away from the horizontal boundaries so that analyses of stability of unidirectional flows will be applicable.

If A/h is greater than a number of order 10^4 and $h \gtrsim 1$, a boundary-layer régime is found with velocity and temperature profiles (Elder 1965*a*; Gill 1966) in the boundary layers, very similar to the profiles under study. It seems likely, therefore, that critical values of the Reynolds number will be of the same order. The vertical temperature gradient found experimentally is approximately $\frac{1}{2}\Delta T/H$, so the boundary-layer width defined in § 2 of the current paper is given approximately by

$$(L/l)^4 = A/8h \tag{7.1}$$

and the Reynolds number R based on this width by

$$(\sigma R)^4 = 2Ah^3. \tag{7.2}$$

Thus if A/h is large enough for the boundary-layer stability analysis to apply, critical conditions will be determined by a value of Ah^3, which is, naturally

enough, just the combination of A and h which is independent of L. Using (7.2) and table 1, the following critical values of Ah^3 are obtained:

$$\begin{aligned} \log(Ah^3) &= 7{\cdot}2 \quad \text{for} \quad \sigma = 0{\cdot}72 \text{ (air)} \\ &= 7{\cdot}3 \quad \text{for} \quad \sigma = 7 \text{ (water)} \\ &= 10{\cdot}4 \quad \text{for} \quad \sigma = 1000 \text{ (oil)}. \end{aligned}$$

The corresponding lines in the (A, h)-plane are shown in figure 17.

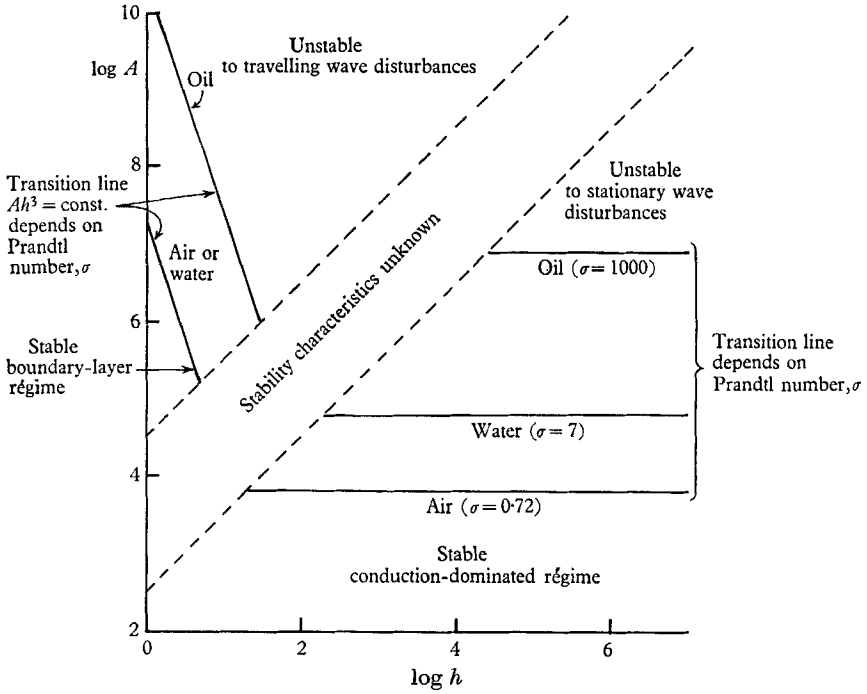

FIGURE 17. Stability characteristics of flow in a vertical slot as a function of Rayleigh number A, aspect ratio h and Prandtl number σ. In the area to the top left of the figure, the basic flow is of the boundary-layer type and becomes unstable to *travelling*-wave disturbances at values of Ah^3 which depend on the Prandtl number. The solid lines represent the approximate values of Ah^3 for Prandtl numbers of 0·72–7 (air or water) and 1000 (oil). In the area to the bottom right of the figure the system is conduction dominated and becomes unstable to *stationary*-wave disturbances at values of A which depend on the Prandtl number. The solid lines represent the appropriate values of A for Prandtl numbers of 0·72 (air), 7 (water) and 1000 (oil). Between the diagonal dotted lines the system is neither conduction dominated nor of the boundary-layer type and the stability characteristics are unknown.

The limiting value of $\log(A/h)$ for which boundary-layer stability analysis can be applied is chosen, rather arbitrarily, as 4·5. This corresponds, by (7.1), to the centre of the slot being at $x_* = 4l$, at which point the velocity fluctuations are still quite significant, as figure 7 shows. The limiting value of $\log(A/h)$ may in fact increase as σ increases since the critical Reynolds number for large σ depends on effects of order $\sigma^{-\frac{1}{2}}$, so that small boundary effects may be significant.

Some results of Rudakov (1967) and Kappus & Lehmann (1965) for small A/h

are also incorporated into figure 17. These results are concerned with the stability of the velocity and temperature field established between infinite parallel vertical plates and are applicable to the slot problem where effects of the upper and lower boundaries are negligible. A/h must be small enough for the basic temperature profile to be approximately linear. The upper limit on $\log A/h$ for this to be true is placed at 2·5 on the basis of the numerical results obtained by Elder (1966).

The stability analysis of Rudakov showed, that for $\sigma < 10$ at least, the first instability to occur is to *stationary* disturbances, rather than to *travelling* disturbances as in the boundary-layer case. The instability appears to be mechanically driven as the critical value of A/σ varies only weakly with σ and is given approximately by

$$\log(A/\sigma) = 3{\cdot}9.$$

The line for $\sigma = 1000$ in figure 17 is based on this formula although Rudakov's analysis did not extend to such large values and, pending further investigation, one should allow for the possibility that some travelling disturbances may prove to be more unstable at very large values of σ.

There appear to be no results either for the middle range of values of A/h given by

$$2{\cdot}5 < \log A/h < 4{\cdot}5.$$

One can hardly extrapolate the results from the two sides as the types of instability and the characters of the equilibria involved are so completely different. It is possible, for instance, that for fixed values of h and σ (say $h = 10$, $\sigma = 1000$) some equilibria corresponding to values of A in the middle range ($3{\cdot}5 < \log A < 5{\cdot}5$) could be unstable, although the boundary-layer equilibrium could be stable at some larger values of A ($5{\cdot}5 < \log A < 7{\cdot}4$ in the case cited).

There is, as yet little experimental evidence with which to compare the results shown in figure 17. Elder quotes three pertinent results but the uncertainties are rather large and the values of A/h tend to be in or close to the middle range. First (Elder 1965*a*, p. 89) he found onset of instability to stationary disturbances for

$$\log A = 5{\cdot}5, \quad \sigma = 1000 \quad \text{and} \quad h = 19,$$

the corresponding value of $\log A/h$ being 4·2, that is, in the middle range. The other two results (Elder 1965*b*, p. 102) are for the onset of instability to travelling disturbances. For $\sigma = 1000$, the appropriate value of Ah^3 is given by

$$\log(Ah^3) = 10{\cdot}4,$$

which happens to be the figure given by the theory for large A/h. However, the corresponding value of A/h is not given. For water ($\sigma = 7$), travelling disturbances were observed when

$$\log(Ah^3) = 9{\cdot}4,$$

a value much higher than the one given by the theory for large A/h. The values of h give a range from 9 to 27 so that $\log(A/h)$ is between 3·7 and 5·6, partly in the middle range. Elder (1965*b*) also remarks on the variation of the critical value

of Ah^3 with σ. In § 5 of the current paper it was found that for $\sigma \to \infty$, the critical Reynolds number varies as $\sigma^{-\frac{1}{2}}$ so, by (7.2),

$$Ah^3 \propto \sigma^2.$$

This differs from the law, suggested by Elder (1965*b*, equation 5).

Comment on the 'double glazing' problem

Figure 17 is of interest in relation to the 'double glazing' problem, that is the problem of choosing for a slot of given height H, a width L which minimizes the heat flux across the vertical boundaries for a given temperature difference ΔT. This problem was discussed by Batchelor (1954). It would appear from figure 17 that if air is the fluid concerned and aspect ratios of 100 or more are involved, the relevant criterion is *not* associated with the change from a conduction-dominated régime to a boundary-layer régime, but is associated rather with the question of whether or not the conduction-dominated system is stable. Clearly the heat transfer across the gap will be enhanced when the system becomes unstable, so L must be chosen so that A is below the critical value, that is,

$$g\Delta T L^3 < 8030\nu^2.$$

If the gap is 1 cm, the system will not become unstable until the temperature difference is around 40 °C. If the gap is 2 cm, the corresponding temperature difference is about 5 °C.

The work of A. Davey was done as part of the general research programme of the National Physical Laboratory.

REFERENCES

Barcilon, V. 1965 *Tellus*, **17**, 53.
Barcilon, V. & Pedlosky, J. 1967 *J. Fluid Mech.* **29**, 609.
Batchelor, G. K. 1954 *Quart. Appl. Math.* **12**, 209.
Benjamin, T. B. 1957 *J. Fluid Mech.* **2**, 554.
Drazin, P. G. & Howard, L. N. 1962 *J. Fluid Mech.* **14**, 257.
Elder, J. W. 1965*a* *J. Fluid Mech.* **23**, 77.
Elder, J. W. 1965*b* *J. Fluid Mech.* **23**, 99.
Elder, J. W. 1966 *J. Fluid Mech.* **24**, 823.
Gershuni, G. Z. 1953 *Zh. Tekh. Fiz.* **23**, 1838.
Gershuni, G. Z. 1955 *Zh. Tekh. Fiz.* **25**, 351.
Gershuni, G. Z. & Zhukhovitzki, E. M. 1958 *Izv. Vyssh. Uchebn. Zavedenii Fiz.* no. 4, 43.
Gill, A. E. 1966 *J. Fluid Mech.* **26**, 515.
Gregory, N., Stuart, J. T. & Walker, W. S. 1955 *Phil. Trans.* A **248**, 155.
Kappus, H. & Lehmann, A. 1965 *Deutsche Luft- und Raumfahrt, Forschungsbericht* 65–15.
Lin, C. C. 1955 *The Theory of Hydrodynamic Stability*. Cambridge University Press.
Lilly, D. K. 1966 *J. Atmos. Sci.* **23**, 481.
Nachtsheim, P. R. 1963 *NASA* TN D-2089.
Polymeropoulos, C. E. & Gebhart, B. 1967 *J. Fluid Mech.* **30**, 225.
Prandtl, L. 1952 *Essentials of Fluid Dynamics*. New York: Hafner.
Rudakov, R. N. 1967 *PMM*, **31**, 367.
Szewczyk, A. A. 1962 *Int. J. Heat Mass Transfer*, **5**, 903.
Veronis, G. 1967 *Tellus*, **19**, 326.